blood

Prepublished online May 26, 2011;
doi:10.1182/blood-2010-09-305383

Loss of *p19Arf* in a Rag1$^{-/-}$ B-cell precursor population initiates acute B-lymphoblastic leukemia

Julia Hauer, Charles Mullighan, Estelle Morillon, Gary Wang, Julie Bruneau, Nicole Brousse, Marc Lelorc'h, Serge Romana, Amine Boudil, Daniela Tiedau, Sven Kracker, Frederick D Bushmann, Arndt Borkhardt, Alain Fischer, Salima Hacein-Bey-Abina and Marina Cavazzana-Calvo

Blood (print ISSN 0006-4971, online ISSN 1528-0020), is published weekly by the American Society of Hematology, 2021 L St, NW, Suite 900, Washington DC 20036.

Loss of *p19Arf* in a Rag1$^{-/-}$ B-cell precursor population initiates acute B-lymphoblastic leukemia

Julia Hauer [1,7], Charles Mullighan [2], Estelle Morillon [1], Gary Wang [3], Julie Bruneau [4], Nicole Brousse [4], Marc Lelorc`h [5], Serge Romana [5], Amine Boudil [6], Daniela Tiedau[7], Sven Kracker[1], Frederic D Bushmann [3], Arndt Borkhardt [7], Alain Fischer[1,8,10], Salima Hacein-Bey-Abina [1,8,9*], Marina Cavazzana-Calvo [1,8,9*].

* contributed equally to this work

1. INSERM U768, René Descartes University of Paris and Necker Children`s Hospital, Paris, France
2. Department of Pathology, St. Jude Children`s Research Hospital, Memphis, USA
3. Department of Microbiology, University of Pennsylvania School of Medicine, Philadelphia, Pennsylvania, USA.
4. Department of Pathology, Necker Children's Hospital, Assistance Publique-Hôpitaux de Paris, René Descartes University of Paris Faculty of Medicine, Paris, France
5. INSERM E0210, René Descartes University of Paris and Necker Children's Hospital, Paris, France
6. INSERM U591, René Descartes University of Paris and Necker Children's Hospital, Paris, France
7. Department of Pediatric Oncology, Hematology and Clinical Immunology, Center for Child and Adolescent Health, Heinrich Heine University, Düsseldorf, Germany
8. Paris Descartes University, Paris, France
9. Biotherapy Clinical Investigation Center, Groupe Hospitalier Universitaire Ouest, Assistance Publique-Hôpitaux de Paris, Paris, France
10. Pediatric Immunology & Haematology Unit, Hôpital Necker Enfants-Malades, Assistance Publique-Hôpitaux de Paris, Paris, France

Corresponding author:

Marina Cavazzana-Calvo, INSERM U768 and Biotherapy Clinical Investigation Center, Hôpital Necker, rue de Sevres 149, F-75015 Paris, France; Tel. +33 144 495246; Fax +33 144 492505; e-mail: sec.biotherapie@nck.aphp.fr; m.cavazzana@nck.aphp.fr

Running Title: Loss of *p19Arf* and *Rag1* initiate B-ALL

Abstract

In human B- acute lymphoblastic leukemia (B-ALL), RAG1-induced genomic alterations are important for disease progression. However, given that biallelic loss of the *RAG1* locus is observed in a subset of cases, RAG1's role in the development of B-ALL remains unclear. We chose a p19Arf$^{-/-}$Rag1$^{-/-}$ mouse model to confirm the previously published results concerning the contribution of CDKN2A (p19Arf /INK4a) and *RAG1* copy number alterations in precursor B-cells to the initiation and/or progression to B-acute lymphoblastic leukemia (B-ALL). In this murine model, we identified a new, Rag1-independent leukemia-initiating mechanism originating from a Sca1+CD19+ precursor cell population and showed that Notch1 expression accelerates the cells' self-renewal capacity *in vitro*. In human Rag1-deficient bone marrow, a similar CD34+CD19+ population expressed *p19Arf*. These findings suggest that combined loss of *p19Arf* and *Rag1* results in B-cell precursor leukemia in mice and may contribute to the progression of precursor B-ALL in humans.

Introduction

Aberrant V(D)J recombination and persistent, non-specific RAG1 endonuclease activity are reportedly key events in the induction of genomic alterations, which contribute to the oncogenic transformation of hematopoietic precursor cells [1]. In contrast *Rag1* deletions have been observed in precursor B-cell leukemia (but not in precursor-T cell leukemia) at a non-insignificant frequency [2]. Because of these partially conflicting results the impact of (i) RAG1 misexpression (leading to leukemogenic DNA cleavage) and (ii) biallelic copy number losses of *RAG1* genes on the initiation or progression of precursor B-ALL remains unclear. There is indirect evidence to suggest that Rag-induced genomic alterations are not essential for leukemia initiation: p53 and non-homologous-end-joining (NHEJ) factor (such as Ku80, DNA-Pkc, Artemis) double-knockout mice develop aggressive pro-B cell leukemia with Rag1-dependent IgH/c-myc translocations [3]. However, in some cases B-ALL still occurs when Rag activity is absent and IgH/c-myc translocation is suppressed [4-7]. Similarly, in an Eμ-c-myc transgenic mouse model, loss of Rag1 increased (rather than suppressed) the incidence of B-cell lymphoma, although the mechanism has not been clarified [8]. Thus, it is likely that both aberrant Rag1 activity and Rag1 deficiency contribute to ALL, albeit with different underlying mechanisms and target cell populations.

In order to study the role of Rag1 loss of function in the initiation of precursor B-ALL, we developed a murine p19Arf$^{-/-}$Rag1$^{-/-}$ double-knockout model. We chose to inactivate these particular genes for two reasons. Firstly, loss of the *RAG1* locus occurs with significant frequency in precursor B-ALL [2], and Rag1 deficiency contributes to leukemogenesis in mouse models only when combined with secondary oncogene activation or tumor suppressor gene inactivation [8,9]. Secondly, *p19ARF* loss-of-function mutations are involved in a high percentage of human precursor B-cell leukemia (16 out of 47 tested cases in [2]). One possible explanation for the predisposition to precursor B-ALL in the absence of RAG1 is that the

Rag-deficiency-induced arrest in B-cell differentiation leads to alterations in the phenotype and frequency of the various lymphoid precursor populations in the bone marrow (BM) [10].

In the present study, we demonstrated that the combined lack of *Rag1* and *p19Arf* results in the emergence of a new subset of Sca1+CD19+ B-cell precursor cells in the BM. This cell fraction contains leukemia initiating cells (LICs) that are specifically characterized by abundant Notch1 expression.

Material and Methods:

Mice

The p19Arf$^{-/-}$ mice were generously provided by Dr Charles Sherr (Saint Jude's Hospital, Memphis, TN, USA) and backcrossed with Rag1$^{-/-}$ mice (Charles Rivers Laboratories, L'Arbresle, France) to obtain p19Arf$^{-/-}$Rag1$^{-/-}$ double-deficient mice. Recipient WT mice were obtained from Charles Rivers Laboratories. RAG2$^{-/-}\gamma c^{-/-}$ animals were generously provided by Dr Jim di Santo (Pasteur Institute, Paris, France). Mice expressed CD45.1 (recipient) or CD45.2 (donor) alloantigens for determination of chimerism in transplantation experiments. Animals were housed in a specific, pathogen-free animal facility at Necker Children's Hospital/René Descartes University, Paris, France. All experiments and procedures were performed in compliance with the French Ministry of Agriculture's Regulations for Animal Experiments (Act 87847, October 19, 1987, as modified in May 2001).

Ex vivo expansion of bone marrow cells and transplantation

Prior to use as donors, mice were closely monitored for pre-existing hematologic abnormalities. Bone marrow was obtained from femurs and tibiae of 4- to 6-week-old mice, red cell blood lysis was performed with 0.75% NH_4Cl solution in tris(hydroxymethyl)aminomethane buffer, Sca1+ cells were selected by labeling with an anti-Sca1-phycoerythrin (PE) antibody (Becton Dickinson, BD Bioscience Pharmingen, San Jose, CA) and subsequent coupling to an anti-PE magnetic selection kit (Miltenyi Biotec, Bergisch Gladbach, Germany).

The Sca1+CD19+ or Sca1+CD19- population was selected by FACS cell sorting. Sca1+CD19- cells were pre-activated for 24 hrs in plates coated with fibronectin (RetroNectin CH-296; Takara Biomedicals, Shiga, Japan) and Stemspan medium supplemented with 5% fetal bovine serum (FBS), 100ng/ml murine stem cell factor (mSCF) (Abcys, Paris, France),

100ng/ml murine FMS-like tyrosine kinase 3-ligand (mFlt3-L) (R&D Systems, Minneapolis, MN, USA), 100ng/ml thrombopoietin (TPO) (R&D Systems), 50ng/ml mIL-6 (Abcys) and 10ng/ml mIL-11 (R&D Systems). Cells were mock-cultured or submitted to three transduction cycles with an MFG-GFP vector at a multiplicity of infection (MOI) of 11. Construction of the MFG-GFP vector and production of viral supernatant has been described elsewhere [11]. A sample of $5x10^5$ "A" or "AR" cells was injected intravenously (i.v.) into 10 Gy-irradiated WT mice. For secondary transplantations, $5x10^6$ leukemic cells from two different AR mice were i.v. transplanted into six non-irradiated $Rag2^{-/-}\gamma c^{-/-}$ animals after red blood cell lysis.

Flow cytometry

Analysis of immunologic reconstitution in “AR” transplanted mice was performed by retro-orbital bleeding 15 weeks after transplantation. Mice were euthanized at the first signs of illness and their thymus, spleen and BM were harvested. Flow cytometry analysis was performed on organs and peripheral blood after red blood cell lysis (Supplementary Material and Methods). Analysis was performed on a FACScalibur machine (BD Biosciences Pharmingen) using Flow Jo software.

Histology

Spleen tissue samples from (i) recipient mice which developed pro-B-cell leukemia, (ii) healthy AR mice and (iii) a WT control mouse were harvested and fixed in phosphate buffered saline (PBS)/10% formalin, embedded in paraffin and cut into 2µm-thick slices. Slides were conventionally stained with hematein-eosin-safran reagent and were interpreted independently by two pathologists (NB and JB).

RT-PCR analysis

cDNA was synthesized using the RNeasy Kit (Qiagen, Hilden, Germany). Primer Sequences, annealing temperatures and fragment size are indicated in the Supplemental Material and Methods (Table S2).

Integration site analysis

Genomic DNA was purified using a phenol-chloroform extraction protocol. Integration site analysis was performed as described elsewhere [12]. In brief, to determine vector integration sites in the mouse genome, DNA fragments from host–vector junctions were prepared using ligation-mediated PCRs. Each DNA sample (1–1.5 mg) was digested with five different enzymes. The digested samples were ligated to linkers and then amplified in nested PCRs. In order to sequence all the samples in a single experiment, primers containing unique 4-base-pair barcodes were used in the second PCR step. The PCR products were gel-purified, pooled and pyrosequenced (454 Life Sciences, Branford, CT, USA).

BrdU incorporation assays

To measure cell proliferation, mice were twice injected intraperitoneally (i.p.) with 1 mg BrdU (Sigma, B5002-1G). Five hours after injection, mice were euthanized and BM was harvested, stained with Sca1+ PE- and CD19 APC-antibodies and fixed in PBS with 0.01% Tween/1% PFA. After a 48-hour incubation, cells were permeabilized in PBS with 0.5% Tween and stained with an anti-BrdU-FITC antibody (Becton Dickinson).

Multiplex PCR

Multiplex RT-PCR analysis was performed according to the method published by Peixoto et al. [13], with some minor modifications. We considered *Mrp-S21* (coding for a protein within

the 28S ribosome subunit) to be a constitutive housekeeping gene. The selected PCR primers are listed in Table S1. Cells were sorted in 96-well plates containing PBS-diethyl pyrocarbonate (Sigma-Aldrich) and stored at –80°C. After cell lysis, RNA was reverse-transcribed using gene-specific 3' primers. The first-round PCR was subsequently performed on the same plate by addition of a premixed PCR buffer containing 3' and 5' primers for all eight genes and operation of 15 cycles. The first-round PCR products were aliquoted into new PCR tubes (2% per second-round PCR). The second-round PCR was performed separately for each individual gene using semi-nested primers (48 cycles). The PCR products were resolved on a 1.5% agarose ethidium bromide gel.

In vitro cell culture assays

Bone marrow was enriched for the CD19+ population using a MACS© magnetic cell sorting kit (Miltenyi Biotec). Subsequently, the $Sca1^{low}ckit^{low}CD19+$ population was sorted by FACS (on a FACSAria machine from Becton Dickinson). For co-culture experiments, sorted cells were cultured on a murine OP-9 stroma cell line expressing (or not) murine Notch-ligand delta1 (OP9-delta1) in alpha MEM (Gibco) supplemented with Hyclone FBS (Perbio), glutamine (Gibco), 2 ng/ml mIL7 (R&D Systems) and 5 ng/ml mFLT3L (R&D Systems). The cells were replated every 7 days. At each replating round cells were washed in PBS and a portion was taken for FACS analysis to establish the expression of B-cell antigens (B220/CD19) or T-cell antigens (CD4/CD8/TCR).

Expression analysis of human *RAG1*$^{-/-}$ bone marrow cells

After the provision of informed consent, BM from a RAG1-deficient patient and a healthy control was isolated. Mononuclear cells were isolated by Ficoll and CD34+ selection was performed using a human CD34 MicroBeadKit (Miltenyi Biotech). The CD34+CD19+ and

CD34+CD19- populations were isolated by FACS and cDNA was synthesized. The Taq-Man primer probe set for the human CDKN2A (p19Arf) locus (assay Hs99999189_m1) was purchased from Applied Biosystems, Courtaboeuf, France.

Statistical analysis

All statistical analyses were performed with GraphPad Prism software (GraphPad Software Inc., La Jolla, CA, USA). Survival was analyzed according to the Kaplan-Meier method and survival curves were compared in a log rank test.

Results

1. A Rag1$^{-/-}$ background and loss of p19Arf act synergistically to promote pro-B-cell leukemia

Double-knockout p19Arf$^{-/-}$Rag1$^{-/-}$ ("AR") mice were born in the anticipated Mendelian proportion. As expected, mature B- and T-cells were totally absent, whereas normal natural killer (NK) monocytes and polynuclear cell counts were observed.

In p19Arf$^{-/-}$ ("A") mice, we observed an overall mortality rate of 50% at 50 weeks after birth. This was mainly due to the development of solid tumors, such as sarcomas and carcinomas. Seventeen percent of the "A" animals developed hematopoietic tumors with a predominantly T-cell phenotype (own data and [14]). "R" mice had an overall survival rate of >90% at 28 weeks after birth [8]. Consistently we did not observe solid or hematopoietic tumors in "R" mice after 52 weeks of follow up in own studies [11]. The overall mortality rate for "AR" mice (65% at 50 weeks) did not differ significantly from that seen in "A" mice. The "AR" mice also developed predominantly solid tumors. Hematologic lymphoproliferation occurred in 26% of "AR" animals but (in contrast to "A" mice) these tumors all had a pro-B-cell phenotype (CD19+IgM-) (Figure 1A and Table 1).

"AR" mice were euthanized as soon as signs of illness were observed. Monomorphic, immature (CD19+IgM-) lymphoblastic proliferation was observed in the BM, liver, spleen, lymph nodes and blood (Figure 1B). Hematein-eosin staining of spleen sections revealed widespread large cell proliferation, with the loss of red/white pulp differentiation. Clusters of large cells with an irregularly bounded nucleus, a prominent nucleolus and numerous partially atypical mitoses were observed (Figure 1C). The "AR" CD19+IgM- population displayed a blastoid phenotype, with surface expression of other B-cell lineage markers (such as BP1,

IL7Rα, B220, CD24 and CD25) (Figure 1D and Figure 1E). We did not detect any residual VDJ recombination or IgH-c-myc/IgH–n-myc translocations, emphasizing the complete absence of Rag1 activity (Figure S1A and Figure S1B).

The occurrence of B-cell precursor leukemia in the "AR" animals suggested a cooperative mechanism involving *Rag1* deficiency and the loss of *p19Arf*.

2. The p19Arf$^{-/-}$Rag1$^{-/-}$ Sca1+ CD19+ population initiates leukemia

The occurrence of pro-B-cell leukemia in this mouse model suggested the existence of a new mechanism capable of inducing Rag1-independent pro-B-cell transformation in hematopoietic progenitors.

To further investigate the Rag1-independent transformation process, we designed a model comprising a 5-day, *ex vivo* expansion of "AR" Sca1+ hematopoietic precursor cells followed by transplantation into lethally irradiated wild type ("WT") mice (Figure 2A). Fifteen weeks later, mixed blood chimerism was observed, with a normal count of donor-derived NK cells (NK1.1: 200/µl), monocytes and polynuclear cells (CD11b: 1500/µl) but given the Rag1 deficiency only low numbers of recipient-derived mature B- and T-cells (CD3+: 350/µl; B220+: 100/µl). As expected, animals transplanted with "A" cells showed full donor chimerism, with normal cell counts in both the lymphoid and myeloid compartments (Figure 2B). With a time to onset of 20-25 weeks post-transplantation, recipients of "AR" cells developed hematopoietic tumors with 100% lethality by 45 weeks post-transplantation. Eighty percent of mice transplanted with "A" cells survived more than 52 weeks ($p<0.0001$). The observed cases of leukemia were predominantly of pro-B-cell origin (90% pro-B, 10% pro-T) in the "AR" transplanted group and were all of T-cell origin in the "A" transplanted

group (Figure 2C and Table 1). Secondary transplantation of the lymphoblastic "AR" CD19+ IgM- pro-B-cells again gave rise to monomorphic infiltration of the spleen, liver and BM in all recipients two weeks after transplantation (Figure S2A). This finding indicated that this lymphoblastic population had a high self-renewal capacity. In view of a possible contribution of ex-vivo culture to the development of leukemia, a cohort of mice was transplanted with non-ex-vivo expanded cells. This cohort showed the same leukemia incidence compared to mice transplanted with ex-vivo-expanded cells (Figure S2B).

The phenotype of the pro-B-cell leukemia derived from the transplanted "AR" mice was identical to that seen in non-transplanted "AR" mice (Figures S2C and Figure S2D) and the gene expression profile of the observed leukemia clustered with the gene expression profile of healthy murine hematopoietic populations in Hardy's fractions B to C. The absence of a BCR-rearrangement was the major criteria to designate the leukemia as pro-B-cell leukemia (Figure S2E). Due to the lack of a BCR-rearrangement we used gamma-retroviral GFP marking of the stem cells and used integration-site tracking as a clonality marker to discriminate a benign polyclonal lymphoproliferation from a monoclonal malignant expansion of lymphoid cells. We transduced "AR" Sca1+ cells with an MFG-green-fluorescent protein (GFP) expressing vector prior to transplantation and observed mono-oligoclonal dominance in the pro-B-cell leukemia. Integration site mapping revealed 1-3 integration sites (Figure 2D). We observed an integration-pattern characteristic of gamma-retroviral vectors (Figure S3A) [12]. The leukemia incidence of a cohort of mice transplanted with transduced cells compared to a cohort of mice transplanted with non-transduced cells revealed no difference. Thus we conclude that the proviral integration does not play a major role in the overall incidence of leukemic events (Figure 2C).

In Rag1-positive human and mouse models of B-ALL, genomic alterations have been shown to be associated with disease progression [1,15]. To assess genomic rearrangements in our

present model, we performed comparative genomic hybridization (CGH) analysis of ten “AR” pro-B-cell leukemias. Chromosome 14 gains were particularly frequent, when compared with cases of B-cell leukemia in Rag1-sufficient models. As expected, Rag1-mediated DNA copy number alterations were absent (Figure S3B).

In light of (i) the leukemic cells' self-renewal capacity, (ii) the lack of genomic alterations and (iii) the fact that the “AR” Sca1+ donor cell population contained 30-40% of CD19+ cells, we decided to investigate the role of a B-cell-committed, LIC population in healthy “AR” BM. To this end, the “AR” Sca1+ donor population was depleted of Sca1+CD19+ cells by cell sorting (Sca1+CD19-). This was followed by *ex vivo* expansion and transplantation into lethally irradiated “WT” mice. The incidence of pro-B-cell leukemia was significantly lower in the recipient mice (60% at 50 weeks post-transplant, n=10) than in a group of animals transplanted with a non-depleted “AR” Sca1+ cell population (100% at 45 weeks post-transplant; $p<0.0003$) (Figure 2E and Table 1). Transduction of the “AR” Sca1+CD19- population with a Rag1-gamma retroviral vector to complement the Rag1 deficiency led to an increase in leukemia frequency and at the same time to a switch in leukemia phenotype from B- to T-cell leukemia. These results indicate that deficiency in *p19Arf* and *Rag1* synergize in the development of pro-B-cell leukemia in this model (Figure 2F).

Conversely, when we directly transplanted the “AR” Sca1+CD19+ population (without prior *ex vivo* expansion) into lethally irradiated “WT” mice, these cells could be tracked in the BM of recipient mice for over 4 months (Figure S4A and Figure S4C). Furthermore, the fact that pro-B-cell leukemia developed one year after transplantation into sublethally irradiated “WT” recipients indicates that the “AR” Sca1+CD19+ cell population has a competitive advantage over “WT” cells (Figure S4B). No donor-derived NK cells (NK1.1), monocytes (CD11b+) and polynuclear cells (Gr1+) were found in the blood of “AR” Sca1+CD19+ transplanted

animals and no donor-derived T-cell precursors were detected in the thymus; these findings clearly show that this population is B-cell lineage-committed and unable to reconstitute the different hematopoietic compartments after transplantation.

3. p19Arf regulates the cell cycle and apoptosis in the "AR" Sca1+CD19+ population

The "AR" Sca1+CD19+ population displayed a high proliferative capacity, as evidenced by 5-bromo-2'-deoxyuridine (BrdU) incorporation assays. In "AR" BM, 45% of the Sca1+CD19+ cells incorporated BrdU, whereas BrdU incorporation rate for the same cell compartment in "WT" and "A" mice was only 10%. Strikingly, an 80% BrdU incorporation rate was seen in the Rag1-deficient Sca1+ CD19+ cells ($p<0.008$ in an unpaired T-test of "AR" vs. "A" and $p < 0.0008$ for R vs. WT). However, loss of *p19Arf* on a $Rag1^{-/-}$ background led to a 3-fold increase in the absolute Sca1+CD19+BrdU+ cell count - probably as a result of impaired cell cycle regulation and the lack of apoptosis induction in the "AR" Sca1+CD19+ population (Figure 3A).

In line with the high cell cycle activity observed in the "AR" and "R" BM populations, we detected co-expression of ckit in the Sca1+CD19+ population in both "AR" and "R" mice ($Sca1^{low}ckit^{low}CD19+$) but not in the vast majority of the corresponding "A" and "WT" animals (Figure 3B). The $Sca1^{low}ckit^{low}CD19+$ cells accounted for 0.9% and 0.6% of the mononuclear cells in "AR" and "R" BM samples, respectively. An absolute 5-fold increase in cell number of the $Sca1^{low}ckit^{low}CD19+$ population was only found in the BM of "AR" mice, compared with "A", "R" and "WT" mice (AR vs. A; $p=0.037$) (Figure 3C). Other B-cell lineage antigens (such as B220, CD24, CD25 and BP1) were expressed at lower levels in the "AR" and "R" population than in the corresponding "A" and "WT" populations; this suggests

that the Sca1^{low}ckit^{low}CD19+ cell population corresponds to an early lymphoid precursor cell, even though CD19 expression determines B-cell lineage commitment.

Despite the phenotypic and proliferative similarities of the "AR" and "R" populations, an absolute increase in cell number and leukemia development was only observed in "AR" mice. In a reverse transcriptase-PCR analysis, we detected *p19Arf* mRNA expression in the cell-sorted Rag1-deficient Sca1^{low}ckit^{low}CD19+ population but not in the "WT" population, suggesting that *p19Arf* has a key role in apoptosis and cell cycle regulation in this specific subpopulation (Figure 3D).

4. Activation of Notch1 signaling in the AR Sca1^{low}cKit^{low}CD19+ population

To further define the developmental stage of the Sca1^{low}ckit^{low}CD19+ population from "AR" mice, a comparative, single-cell, multiplex PCR analysis of fluorescence-activated cell sorting (FACS)-sorted Sca1^{low}ckit^{low}CD19+ cells was performed in "AR", "A", "R" and "WT" mice. Important transcription factors for B-cell commitment or cytokine receptors were found to be expressed with similar frequencies in the "AR" Sca1^{low}ckit^{low}CD19+ population (*Il7ra*:85%; *E2a*:88%) and the corresponding "R" population (*Il7ra*:72%; *E2a*:82%). The expression frequencies were lower in the corresponding "A" (*Il7ra*:52%; *E2a*:72%) and "WT" populations (*Il7ra*:40%; *E2a*:67%). However, *Pu1* was expressed to a greater extent in "AR" and "R" cells (50% and 69%, respectively) than in "A" and "WT" cells (24% and 20%, respectively). *Notch1* was found to be expressed with frequencies of 64%, 49%, 18% and 17% in the Sca1^{low}ckit^{low}CD19+ cells from "AR", "R", "A" and "WT" mice, respectively. These values indicate that "AR" and "R" cells harbor the characteristics of earlier progenitors with a broader differentiation capacity. In contrast, other early hematopoietic lineage

transcription factors (such as *Lmo2* or *Gata1*) were expressed at similar frequencies in all analyzed cells. The myeloid lineage-specific transcription factor *Gmcsfr* and the T-lymphoid specific factor *Gata3* were expressed in less than 5% of all tested cells (Figure 4A).

The high frequency of *Notch1* detection in the Rag1-deficient Sca1^{low}ckit^{low}CD19+ population also suggested early hematopoietic characteristics and prompted us to test activation of the *Notch1* signaling pathway in this population. An RT-PCR analysis revealed marked *Hes1* transcription in the pro-B-cell tumors (AR*) and the "AR" Sca1^{low}ckit^{low}CD19+ population but to a lesser extent in the "A", "R" and "WT" populations; this clearly indicates the transcription of *Notch1* downstream target genes (Figure 4B). We next decided to study the population's Notch1-Notch-ligand mediated differentiation capacity by performing co-cultures on a stroma cell line expressing Notch-ligand delta-1 (OP-9-delta-1). "AR" cells expanded and expressed CD19+ for more than 50 days when co-cultured on an OP-9-delta1-expressing stroma cell line, whereas CD19-expressing cells derived from "A" and "WT" populations were not detectable 10-14 days after the start of co-culture (Figure 4C and Figure 4D). In order to determine whether the observed proliferative effect was really due to activation of Notch1-Notch-ligand signaling pathway, or rather to cytokine supplementation, cells were plated on OP-9 or OP-9-delta-1 cell-lines supplemented with the same cytokines (mFlt3L and mIL7). For the "AR" population, a higher proliferation index was observed when the cells were plated on OP-9-delta-1, compared with OP-9 (Figure S5B). Additionally in the presence of a Notch1 signalling pathway inhibitor (γ-secretase inhibitor) the proliverative effect of the „AR" population on OP-9-delta-1 was diminished, indicating the importance of active Notch1 signalling for the selfrenewal capacity of the cells. (Figure S5A). It is noteworthy, when "AR" cells were cultured on OP-9-delta1 stroma the cells did not generate any DN3 T-cell precursors. Thus activation of the Notch1 signaling pathway induces proliferation and not differentiation in this population. This particular "AR"

subpopulation formed morphologically B-cell-like colonies in semi-solid medium and the colonies could be replated for up to 120 days (compared with 40 and 20 days for “A” and “WT” populations, respectively; data not shown).

The fact that (i) *Hes1* was highly expressed in the “AR” population, (ii) Notch1-Notch-ligand interaction led to increased proliferation and (iii) co-culture on OP-9-delta-1 stroma did not lead to down-regulation of CD19 and apoptosis induction, indicates that Notch1-Notch-ligand interaction mediates a proliferative signal and not a differentiation signal in the “AR” population. This effect thus contributes to the cells' extended self-renewal capacity.

5. CD34+CD19+ population with high *p19Arf* expression in the human Rag1 deficiency.

We next sought to identify a corresponding population in the BM of $Rag1^{-/-}$ patients and so harvested mononuclear cells (MNCs) from the BM of RAG1-deficient patients. We observed the accumulation of a CD34+CD19+ population in these patients, when compared with MNCs harvested from BM of a healthy individual (Figure 5A). Quantitative RT-PCR using a commercially available p19Arf probe revealed 26-fold higher expression of *p19Arf* in the $Rag1^{-/-}$ CD34+CD19+ compartment than in the CD34+CD19- compartment; this finding suggests that p19Arf expression also has an important role in this human $Rag1^{-/-}$ CD34+CD19- population (Figure 5B).

Discussion

Persistent Rag1 activity and the resulting genomic alterations have been frequently described and are thought to be part of an important mechanism in the acquisition of genomic alterations which contribute to the development of murine and human B-ALL [1,2]. However, there is still debate as to whether the decisive trigger for transformation of hematopoietic precursors into B-ALL is the type and frequency of Rag1-induced genomic alterations or the nature of the target population itself. Thus the phenotype of BCR-ABL-positive leukemia depends not only on expression of the fusion protein itself but also on the molecular characteristics of the target hematopoietic precursor population [15-17].

Here, we described a new Rag1-independent B-ALL initiation mechanism by using a p19Arf$^{-/-}$Rag1$^{-/-}$ "AR" double-knockout mouse model. The hematopoietic tumors occurring in "AR" mice were exclusively cases of pro-B-cell leukemia, which contrasted with the situation in "A" mice (T-cell leukemia only) and "R" mice (no tumors) [8,11]. Transplantation experiments identified a very rare "AR" Sca1+CD19+ population as the LICs. The population's surface antigen expression pattern as well as the populations transcription profile (as measured in single-cell, multiplex PCR assays) is characteristic of both the B-lineage committed cells (such as *Il7ra* and *E2a)* and the early lymphoid progenitor (ELP) to common lymphoid progenitor (CLP) transition (such as *Pu1* and *Notch1*) [18 19]. This is consistent with earlier findings indicating that lymphoid LICs do not follow the same cellular hierarchy as their physiological counterparts [20].

Activation of the *Notch1* signaling pathway inhibits B-cell differentiation and down-regulates CD19 during lymphoid precursor differentiation as we demonstrated for the "A" and "WT" populations and as previously described [19,21-23]. Expression of *Notch1* on the "AR" Sca1^{low}ckit^{low}CD19+ population led to activation of the Notch1 signaling pathway in the "AR" cells, as shown by (i) the expression of the prototypic *Notch1* target gene *Hes1* [24] and

(ii) their extended self renewal capacity when co-cultured with OP-9-delta-1 stroma cells but not on OP-9 stromal cells as well as their diminished self renewal capacity when a Notch1 signalling inhibitor is added to culture, despite the continued expression of CD19 antigen. It is noteworthy that this "AR" population was B-lineage-restricted in transplantation experiments and was thus unable to reconstitute other hematopoietic cell lineages. Nevertheless the population was able to engraft recipients long term as shown in transplantation experiments and this is consistent with results obtained from repopulating assays on methocult. Moreover, a new study has recently demonstrated the importance of *Notch1* expression and activation of the Notch1-Notch ligand-signaling pathway for the self-renewal capacity and for the long-term engraftment of HSCs. The engraftment is dependent on the expression of specific homing molecules such as VE-cadherin, VEGFR2 and Notch-Notch ligand interaction [25]. Taken as a whole, our results support a role of Notch-Notch ligand interaction for longterm-engraftment and extended repopulating capacity of a pre-leukemic "AR" $Sca1^{low}ckit^{low}$ CD19+ population. However it is still of debate whether activation of Notch1 signaling pathway in an outgrown B-ALL has a different effect. Kannan et al recently reported a suppressive effect of Notch1 activation using a cell line system of B-ALL. This can be indicative of Notch1 providing different effects at the timepoint of initiation and maintenance of leukemia. Further experiments will be necessary to declare the role of Notch1 at different stages of leukemia development [26]

The corresponding $Sca1^{low}ckit^{low}$CD19+ Rag1-deficient B-precursor population expressed *p19Arf*. Signer et al. have described the expression of *p19Arf* in B-precursor cells at the CLP to pre-B-cell stage in young "WT" mice [27]. Our present results suggest that $Rag1^{-/-}$ early B-cell precursors are at a developmental stage in which precise control of the p19Arf-MDM2-p53 axis is needed to regulate the cell cycle and apoptosis since loss of *p19Arf* in a Rag1-deficient B-cell precursor subset is enough to drive B-ALL development at a high frequency.

Additionally the shift in hematopoetic cell populations in the bone marrow with the accumulation of a CD19+-precursor population is an explanation for the switch in leukemia phenotype from T- in "A" mice to pro-B-cell leukemia in "AR" mice. The fact that gamma retroviral correction of Rag1 deficiency in the AR Sca1+CD19- population led to a decrease in the incidence of pro-B-cell leukemia supports the presence of synergy between the loss of *p19Arf* and loss of Rag1 in this pre-leukemic subpopulation. It will be interesting to confirm the strength of this pathway in a $Rag1^{-/-}$ mouse model with conditional, B-cell-specific loss of *p19Arf*.

Translation of the $Sca1^{low}ckit^{low}$CD19+ population to the human hematopoietic system is difficult because the Sca1+ antigen does not exist in the human stem cell nomenclature. However, CD34+ is expressed on human stem cells and lymphoid precursor cells in a similar way to the Sca1 antigen in the murine HSC compartment. Interestingly, we found that a CD34+CD19+ population accumulated in Rag1-deficient patients. This population was previously described as co-expressing CD36, the pan-B-cell markers CD22 and CyCD79a - none of which have been detected in healthy individuals [10]. We demonstrated higher levels of *p19Arf* expression in this human $Rag1^{-/-}$ CD34+CD19+ cell subset than in the less mature CD34+CD19- population, indicating that *p19Arf* also plays an important role in the cell cycle control in the human $Rag1^{-/-}$ CD34+CD19+ population. The functional characteristics of this human precursor have not yet been studied and a predisposition to leukemia (even years after allogeneic stem cell transplantation) in Rag1-deficient patients has not been reported. However, the data from our new murine model parallels the hypothesis put forward by Greaves et al, whereby a CD34+CD38-CD19+ population that is absent from healthy individuals can be detected in patients with TEL/AML1 positive B-cell precursor leukemia [28,29]. In addition, genomic alterations involving losses of the Rag1 locus were described in 16% of a cohort of 50 TEL/AML1-positive patients [30]. In contrast mutations in the Rag1 locus

in T-cell leukemia were absent. These Rag1 mutations are often monoallelic on diagnosis and become biallelic at relapse - indicating a possible selective advantage of Rag1-deficient cells in the progression of B-ALL[2].

Further opportunities will involve characterizing *NOTCH1* signaling in the human Rag1$^{-/-}$ CD34+CD19+ population by knock-down of *p19ARF* expression and transplantation into a NOD-SCID xenograft model. This will shed light on the role of *NOTCH1* in the process of B-ALL initiation.

Acknowledgements

We thank Dr Brian Sorrentino and Albert Zhou for valuable discussions on murine p19Arf models, Dr Isabelle Andre-Schmutz, Dr Chantal Lagresle-Peyrou, Eva-Maria Weick and Julie Riviere for helpful discussions and advice, Dr Charles Sherr (Saint Jude's Hospital, Memphis TN, USA) for providing p19Arf$^{-/-}$ mice and Dr Jim di Santo (Pasteur Institute, Paris) for providing Rag2$^{-/-}\gamma C^{-/-}$ mice. We also thank Amelyne David and Julie Piquet for animal work.

JH was funded by a fellowship from the Akademie der Naturforscher Leopoldina (BMBF-LPD 9901/8-149) and the "Strategischer Forschungsfond" of the Heinrich-Heine-Unversity Düsseldorf, Germany. MCC was funded by grants from INSERM, the Consert contract #005242 and the Agence Nationale de la Recherche (ANR) grant 05-MRAR-004. FDB was supported by NIH grants AI52845 and AI66290 to FDB. GPW was funded by NIH NIAID T32 AI07634 (Training Grant in Infectious Diseases) and the University of Pennsylvania SOM Department of Medicine Measey Basic Science Fellowship Award.

Authorship Contributions and Disclosure of Conflicts of Interest

JH and EM designed the p19Arf$^{-/-}$Rag1$^{-/-}$mouse model, performed transplantation experiments and analysed the tumours. CM performed CGH-analysis and Affymetrix expression analysis

of mouse tumours. JH and AB performed Multiplex-PCR analysis. SR and ML performed FISH analysis. JH, GW and RB performed integration site analysis. JB and NB performed histology. DT performed expression analysis. SK contributed with scientific advice and discussions. JH, SHBA, AB, AF and MCC designed experiments and wrote the manuscript.

All authors declare no conflicts of interest.

References

1. Mullighan CG, Goorha S, Radtke I, et al. Genome-wide analysis of genetic alterations in acute lymphoblastic leukaemia. *Nature*. 2007;446(7137):758-764.

2. Mullighan CG, Phillips LA, Su X, et al. Genomic analysis of the clonal origins of relapsed acute lymphoblastic leukemia. *Science.* 2008;322(5906):1377-1380.

3. Lieber MR, Yu K, Raghavan SC. Roles of nonhomologous DNA end joining, V(D)J recombination, and class switch recombination in chromosomal translocations. *DNA Repair (Amst).* 2006;5(9-10):1234-1245.

4. Difilippantonio MJ, Zhu J, Chen HT, et al. DNA repair protein Ku80 suppresses chromosomal aberrations and malignant transformation. *Nature.* 2000;404(6777):510-514.

5. Gladdy RA, Taylor MD, Williams CJ, et al. The RAG-1/2 endonuclease causes genomic instability and controls CNS complications of lymphoblastic leukemia in p53/Prkdc-deficient mice. *Cancer Cell.* 2003;3(1):37-50.

6. Vanasse GJ, Concannon P, Willerford DM. Regulated genomic instability and neoplasia in the lymphoid lineage. *Blood.* 1999;94(12):3997-4010.

7. Zhu C, Mills KD, Ferguson DO, et al. Unrepaired DNA breaks in p53-deficient cells lead to oncogenic gene amplification subsequent to translocations. *Cell.* 2002;109(7):811-821.

8. Nepal RM, Zaheen A, Basit W, Li L, Berger SA, Martin A. AID and RAG1 do not contribute to lymphomagenesis in Emu c-myc transgenic mice. *Oncogene*. 2008;27(34):4752-4756.

9. Nacht M, Jacks T. V(D)J recombination is not required for the development of lymphoma in p53-deficient mice. *Cell Growth Differ*. 1998;9(2):131-138.

10. Noordzij JG, de Bruin-Versteeg S, Verkaik NS, et al. The immunophenotypic and immunogenotypic B-cell differentiation arrest in bone marrow of RAG-deficient SCID patients corresponds to residual recombination activities of mutated RAG proteins. *Blood.* 2002;100(6):2145-2152.

11. Lagresle-Peyrou C, Yates F, Malassis-Seris M, et al. Long-term immune reconstitution in RAG-1-deficient mice treated by retroviral gene therapy: a balance between efficiency and toxicity. *Blood*. 2006;107(1):63-72.

12. Wang GP, Garrigue A, Ciuffi A, et al. DNA bar coding and pyrosequencing to analyze adverse events in therapeutic gene transfer. *Nucleic Acids Res.* 2008;36(9):e49.

13. Peixoto A, Monteiro M, Rocha B, Veiga-Fernandes H. Quantification of multiple gene expression in individual cells. *Genome Res.* 2004;14(10A):1938-1947.

14. Kamijo T, Bodner S, van de Kamp E, Randle DH, Sherr CJ. Tumor spectrum in ARF-deficient mice. *Cancer Res.* 1999;59(9):2217-2222.

15. Mullighan CG, Williams RT, Downing JR, Sherr CJ. Failure of CDKN2A/B (INK4A/B-ARF)-mediated tumor suppression and resistance to targeted therapy in acute lymphoblastic leukemia induced by BCR-ABL. *Genes Dev.* 2008;22(11):1411-1415.

16. Wang PY, Young F, Chen CY, et al. The biologic properties of leukemias arising from BCR/ABL-mediated transformation vary as a function of developmental origin and activity of the p19ARF gene. *Blood.* 2008;112(10):4184-4192.

17. Williams RT, den Besten W, Sherr CJ. Cytokine-dependent imatinib resistance in mouse BCR-ABL+, Arf-null lymphoblastic leukemia. *Genes Dev.* 2007;21(18):2283-2287.

18. Hardy RR, Hayakawa K. B cell development pathways. *Annu Rev Immunol.* 2001;19:595-621.

19. Nutt SL, Kee BL. The transcriptional regulation of B cell lineage commitment. *Immunity.* 2007;26(6):715-725.

20. le Viseur C, Hotfilder M, Bomken S, et al. In childhood acute lymphoblastic leukemia, blasts at different stages of immunophenotypic maturation have stem cell properties. *Cancer Cell.* 2008;14(1):47-58.

21. Cobaleda C, Schebesta A, Delogu A, Busslinger M. Pax5: the guardian of B cell identity and function. *Nat Immunol.* 2007;8(5):463-470.

22. Maillard I, Fang T, Pear WS. Regulation of lymphoid development, differentiation, and function by the Notch pathway. *Annu Rev Immunol.* 2005;23:945-974.

23. Tanigaki K, Honjo T. Regulation of lymphocyte development by Notch signaling. *Nat Immunol.* 2007;8(5):451-456.

24. Kojika S, Griffin JD. Notch receptors and hematopoiesis. *Exp Hematol.* 2001;29(9):1041-1052.

25. Butler JM, Nolan DJ, Vertes EL, et al. Endothelial cells are essential for the self-renewal and repopulation of Notch-dependent hematopoietic stem cells. *Cell Stem Cell*;6(3):251-264.

26. Kannan S, Fang W, Song G, et al. Notch/HES1-mediated PARP1 activation: a cell type-specific mechanism for tumor suppression. *Blood;*117(10):2891-2900.

27. Signer RA, Montecino-Rodriguez E, Witte ON, Dorshkind K. Aging and cancer resistance in lymphoid progenitors are linked processes conferred by p16Ink4a and Arf. *Genes Dev.* 2008;22(22):3115-3120.

28. Greaves MF. Stem cell origins of leukaemia and curability. *Br J Cancer.* 1993;67(3):413-423.

29. Hong D, Gupta R, Ancliff P, et al. Initiating and cancer-propagating cells in TEL-AML1-associated childhood leukemia. *Science.* 2008;319(5861):336-339.

30. Mullighan CG, Su X, Zhang J, et al. Deletion of IKZF1 and prognosis in acute lymphoblastic leukemia. *N Engl J Med.* 2009;360(5):470-480.

				hematopoietic tumours		
Donor	**Population**	**Treatment**	**Recipient**	**%**	**B-cell**	**T-cell**
AR n=19	-	-	-	26	5/19	0/19
AR n=11	Sca1+	mock	WT	100	10/11	1/11
AR n=12	Sca1+	GFP	WT	100	10/12	2/12
AR n=10	Sca1+CD19-	GFP	WT	60	4/10	2/10
AR n=8	Sca1+CD19-	Rag1	WT	88	2/8	5/8
A n=17	-	-	-	17	0/17	3/17
A n=9	Sca1+	mock	WT	11	0/9	1/9
A n=9	Sca1+	GFP	WT	22	0/9	2/9

Table 1. Characteristics of the mouse cohorts. Numbers of mice are indicated for each group used in this study, along with the donor population, *ex vivo* treatments, the percentage of animals having developed hematopoietic tumors and the tumor phenotype.

Figure legends

Figure 1. **Phenotype of pro-B-cell leukemia in "AR" mice.** "AR" and "A" mice were kept in a pathogen-free animal facility and were euthanized at the first signs of illness. (**A**) Kaplan-Meier analysis of overall survival as a % of "AR" mice (◊, n= 19) and "A" mice (■, n= 17) without any treatment over a 52-week follow-up period post-birth. A log-rank test was used to compare survival in the two cohorts ($p<0.3887$). **(B)** Macroscopic splenomegaly in diseased AR* mice, compared with spleens of healthy, age-matched "A", "AR", "WT" and "R" mice, as well as a CD19+IgM- cell population as the percentage of total MNCs in the spleen and bone marrow (BM) of diseased "AR" mice ("AR*") and age-matched healthy AR mice. **(C)** Hematein-eosin staining of spleen sections from an "AR*" mouse, an age-matched healthy "AR" mouse and a "WT" mouse at 100x and 400x magnification. Lymphoblast infiltration (*) and atypical mitoses (**) are present in the "AR*" spleen sections. Normal, extramedullar hematopoiesis showing erythroblasts and megakaryocytes is present in the healthy "AR" and "WT" mice. **(D)** Fluorescence-activated cell sorting (FACS) analysis of BM and spleen from a diseased "AR*" mouse and healthy, age-matched "AR" and "WT" mice gated on the white blood cell (WBC) populations after red blood cell lysis. Dot plots indicate the percentage of the immature lymphoblastoid CD19+IgM- ("AR*"), healthy immature CD19+IgM- ("AR") and mature CD19+IgM+ ("WT") B-cell compartments in the spleen and the immature (CD19+IgM-) populations in the BM of the indicated mice, respectively. **(E)** Histograms indicate the surface expression (according to an immunofluorescence analysis) of IL7Rα, CD25, BP1, CD24 and B220 gated on the CD19+IgM- population of an "AR" pro-B-cell leukemia sample from the spleen.

Figure 2. Transplantation of the "AR" Sca1+CD19+ population results in leukemia. (A) Experimental design. Hematopoietic stem cells (HSCs) (CD45.2) were cultured *ex vivo* for 5 days in the presence of mSCF, mTPO, mFLT3L, mIL6 and mIL11 (with or without gamma retroviral (MFG-GFP) transduction) and then transplanted into 10 Gy-irradiated WT mice (CD45.1). (**B**) A blood chimerism analysis of recipient animals 15 weeks after transplantation on the basis of CD45.1 (recipient) and CD45.2 (donor) alloantigen expression. The T-cell (CD3+), B-cell (B220+), NK-cell (NK1.1+) and monocyte (CD11b+) subpopulations were analyzed by immunofluorescence. (■) indicates the white blood cell count/µl (WBC) and (□) indicates the CD45.2 + cell count/µl in the blood. Columns represent the mean values and standard deviations for "AR" mice (n=11) and "A" mice (n=9). **(C)** Kaplan-Meier survival curves of "WT" mice transplanted with "A"-derived Sca1+ mock-transduced (Δ, n=9) and GFP-transduced cells (▲, n=9) or "AR"-derived Sca1+ mock-transduced (□, n=11) and MFG-GFP vector-transduced cells (■, n=12). A log-rank test was used to compare the groups ($p<0.0001$). **(D)** Integration site analysis of pro-B-cell leukemia in the "AR-GFP" cohort. Gel electrophoresis of polymerase chain reaction (PCR)-amplified genomic vector integration fragments showed a polyclonal integration pattern for the "AR-GFP" Sca1+ (Sca1+) pool before transplantation (lanes S1 and S2) and a characteristic, mono-oligoclonal integration pattern found in seven transduced "AR" pro-B-cell tumors ("AR*") (lanes 1,4,5,9,12,13,1x); M represents the DNA ladder. (**E**) "AR" Sca1+CD19- GFP-transduced cells were transplanted into lethally irradiated WT recipients. The Kaplan-Meier curve shows a significantly (*) lower incidence of B-cell leukemia in mice transplanted with the "AR" Sca1+CD19- population (black ■, n=10) than in animals transplanted with the "AR" Sca1+ population (dashed ■, n=12, $p<0.0003$ in a log rank test) at 52 weeks post-transplantation. **(F)** Kaplan-Meier survival curves of "WT" mice transplanted with "AR"-derived Sca1+CD19- GFP transduced-cells (n=12), "AR"-derived Sca1+CD19- Rag1 transduced cells (n=8).

Figure 3. Role of p19Arf in the Rag1-deficient Sca1+ CD19+ population. (A) BrdU incorporation is shown both as a percentage of the Sca1+CD19+ population and as a cell count ($x10^3$) (Sca1+CD19+BrdU+). The FACS histograms show the mean level of BrdU incorporation in % by the Sca1+CD19+ population (n=3). (**B)** The histograms indicate ckit expression gated on the Sca1+CD19+ population in "AR", "A", "R" and "WT" bone marrow (BM) in an immunofluorescence analysis. One of four representative experiments is shown here. (**C**) Frequency (%) and absolute cell numbers ($x10^5$) of $Sca1^{low}$ $ckit^{low}$ CD19+ cells in "AR", "A", "R" and "WT" BM ($p<0.037$ for "AR" vs. "A"; n=4) is indicated. (**D**) cDNA was synthesized from BM-derived "R" and "WT" flow-sorted $Sca1^{low}ckit^{low}$CD19+ cells. After 5-fold dilution of the cDNA, RT-PCR assays were used to analyze expression of *p19Arf* and the control housekeeping gene actin. One of three representative experiments is shown here.

Figure 4. Transcriptional profiles and the role of Notch-Notch-ligand interaction in the "AR" and "R" populations. The AR $Sca1^{low}$ $ckit^{low}$ CD19+ population was flow-sorted from "AR", "A", "R" and "WT" bone marrow (BM). (**A**) Between 30 and 40 single cells (60 for "R") from the $Sca1^{low}ckit^{low}$CD19+ population from "AR" (black), "A" (white), "R" (dark grey) and "WT" (light grey) BM were sorted into 96-well plates. Single-cell RT-PCR analysis was performed for the early hematopoietic genes *Lmo2* and *Gata1*, the B-cell lineage genes *Pu1*, *Il7rα* and *E2a*, the cell cycle genes *Runx1* and *c-myB* and the gene for the T-cell transcription factor *Notch1*. The figure illustrates positive gene expression in terms of the percentage of analyzed cells. *Mrp-S21* served as an internal control, PBS-loaded wells with no cells served as a negative control and both controls were run for all primer sets. The data shown come from two independent cell preparations and RT-PCR experiments. An asterisk (*) indicates a statistically significant difference. (**B**) RT-PCR of the prototypic *Notch1* target gene *Hes1*, using equal amounts of cDNA in two pro-B-cell tumors AR*, in the healthy

FACS-sorted Sca1^{low}ckit^{low}CD19+ "AR", "A", "R" and "WT" populations and in the thymus of a WT mouse (T). One of three experiments (with two independent cell preparations) is shown**. (C)** Sca1^{low}ckit^{low}CD19+ populations from "AR", "A" and "WT" mice were co-cultured on an OP-9 stroma cell line expressing murine Notch-ligand delta1 (OP-9-delta-1) in the presence of mFlT3L and mIL7. Cells were replated every week for >40 days. Shown is one representative experiment out of two. **(D)** The histograms show the CD19 expression at days 8 (D8) and 33 (D33). One of three representative experiments is shown.

Figure 5. *p19ARF* expression in the human Rag1$^{-/-}$ CD34+CD19+ population

(A) FACS analysis of a Rag1-deficient patient after CD34+ cell sorting of bone marrow-derived MNCs (one of six representative experiments is shown here). **(B)** Taq-Man analysis of *p19ARF* expression in the cell-sorted human RAG1$^{-/-}$ CD34+CD19+ and CD34+CD19- population indicated 26-fold higher *p19ARF* expression in the CD34+CD19+ population than in the CD34+CD19- counterpart. One of two independent Taq-Man analysis of a patient sample is shown here.

Figure 1

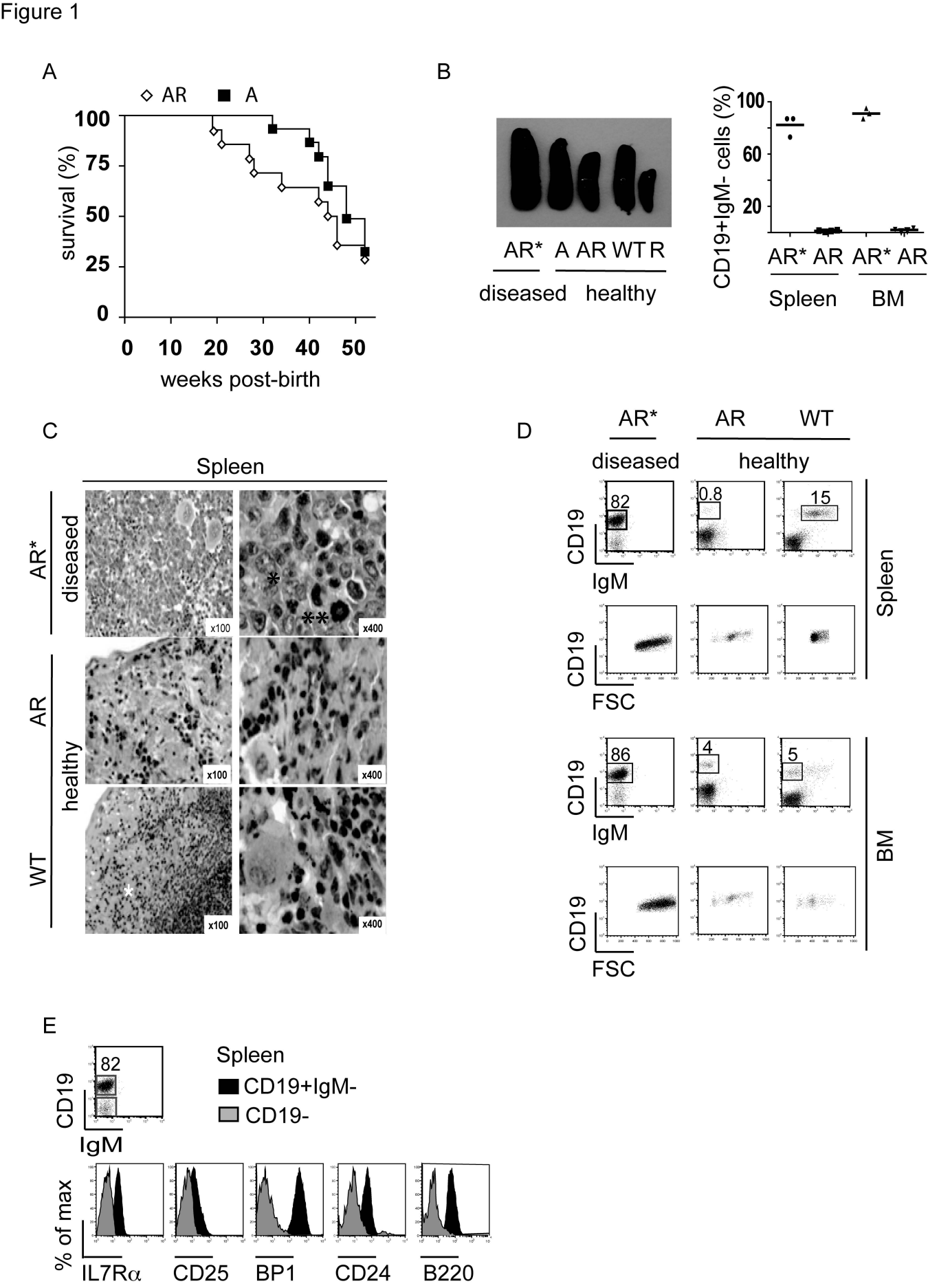
A
AR
A
100
75
50
25
0
survival (%)
0 10 20 30 40 50
weeks post-birth
B
AR* A AR WT R
diseased healthy
CD19+IgM- cells (%)
100
60
20
AR* AR AR* AR
Spleen BM
C
Spleen
AR*
diseased
AR
healthy
WT
x100
x400
D
AR*
AR
WT
diseased
healthy
CD19
IgM
FSC
82
0.8
15
86
4
5
Spleen
BM
E
Spleen
CD19+IgM-
CD19-
82
CD19
IgM
% of max
IL7Rα
CD25
BP1
CD24
B220

Figure 2

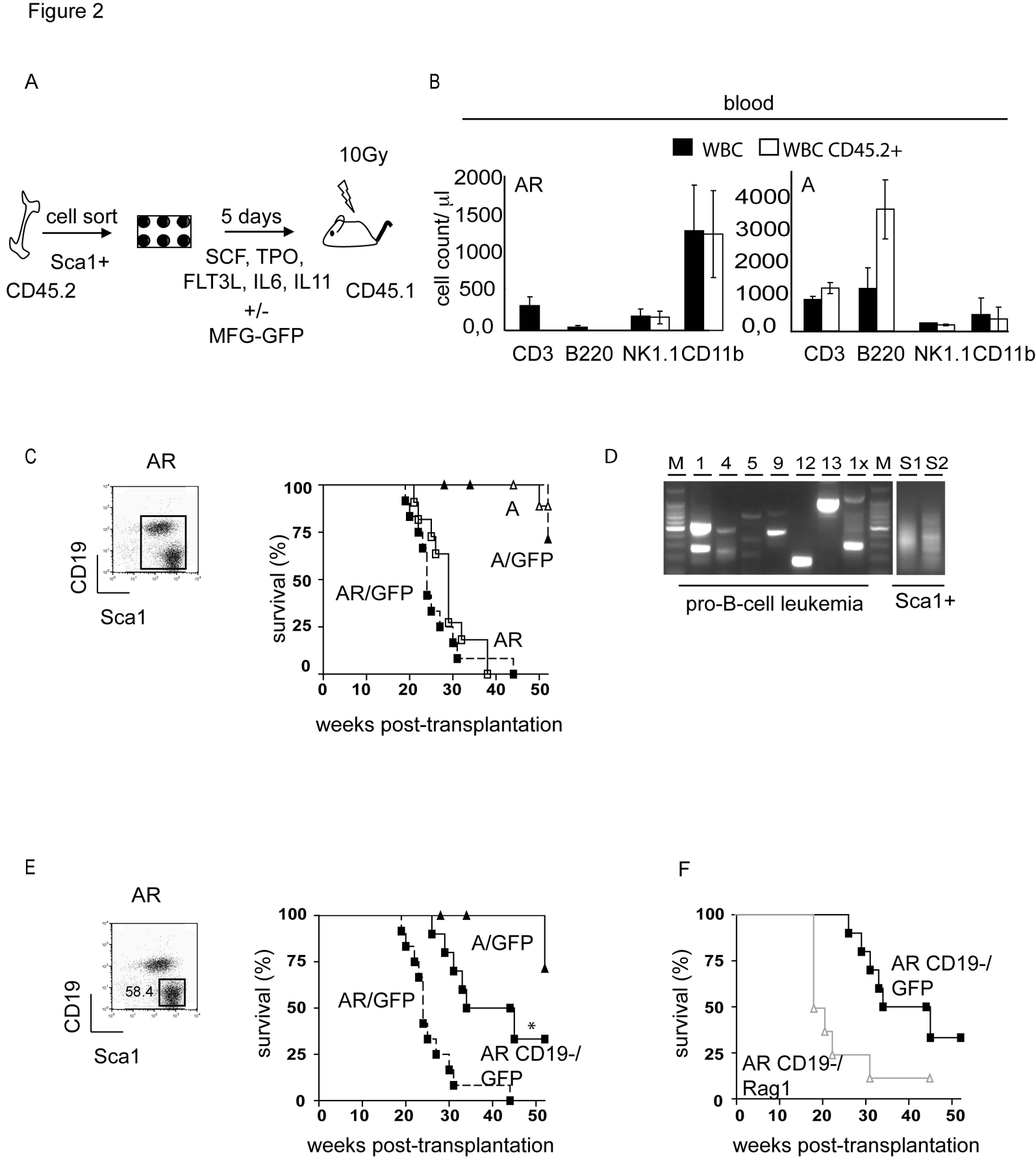
A
cell sort
Sca1+
CD45.2
5 days
SCF, TPO,
FLT3L, IL6, IL11
+/-
MFG-GFP
10Gy
CD45.1
B
blood
WBC
WBC CD45.2+
cell count/ µl
AR
A
CD3 B220 NK1.1 CD11b
C
AR
CD19
Sca1
survival (%)
A
A/GFP
AR/GFP
AR
weeks post-transplantation
D
M 1 4 5 9 12 13 1x M S1 S2
pro-B-cell leukemia
Sca1+
E
AR
CD19
58.4
Sca1
survival (%)
A/GFP
AR/GFP
AR CD19-/
GFP
weeks post-transplantation
F
survival (%)
AR CD19-/
GFP
AR CD19-/
Rag1
weeks post-transplantation

Figure 3

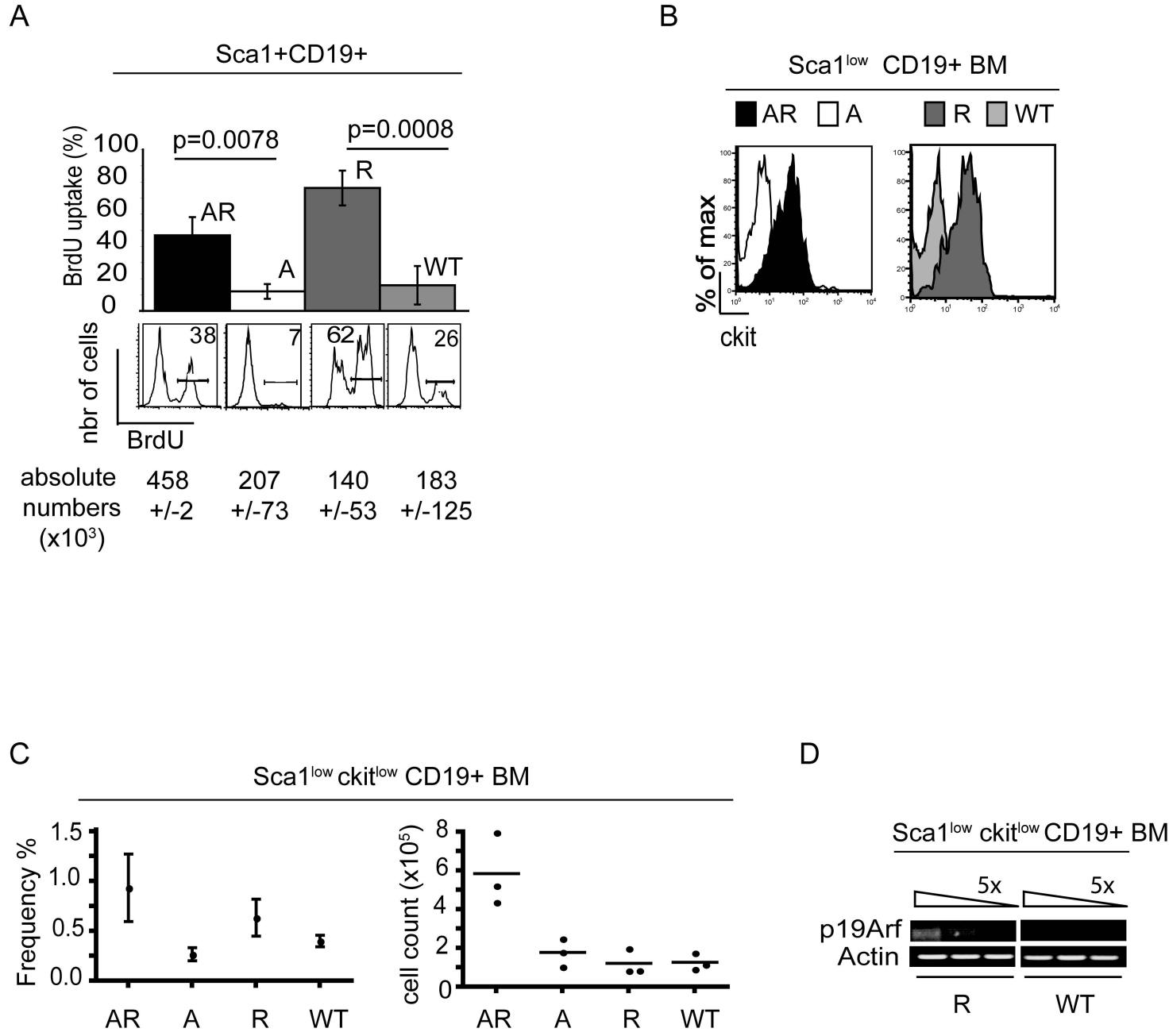
A
Sca1+CD19+
p=0.0078
p=0.0008
BrdU uptake (%)
100
80
60
40
20
0
AR
A
R
WT
nbr of cells
38
7
62
26
BrdU
absolute numbers (x10³)
458 +/-2
207 +/-73
140 +/-53
183 +/-125
B
Sca1low CD19+ BM
AR
A
R
WT
% of max
ckit
C
Sca1low ckitlow CD19+ BM
Frequency %
1.5
1.0
0.5
0.0
AR
A
R
WT
cell count (x10⁵)
8
6
4
2
0
AR
A
R
WT
D
Sca1low ckitlow CD19+ BM
5x
5x
p19Arf
Actin
R
WT

Figure 4

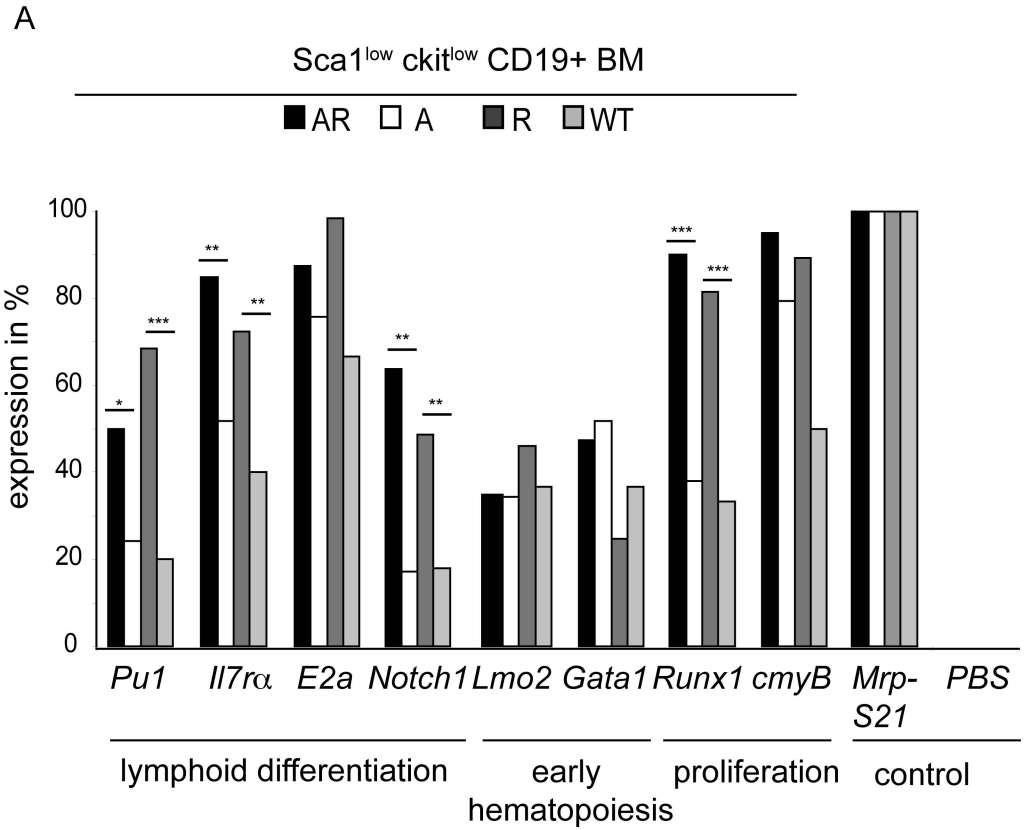
A
Sca1low ckitlow CD19+ BM
AR
A
R
WT
expression in %
100
80
60
40
20
0
*
***
**
**
**
**
***
***
Pu1
Il7rα
E2a
Notch1
Lmo2
Gata1
Runx1
cmyB
Mrp-S21
PBS
lymphoid differentiation
early hematopoiesis
proliferation
control

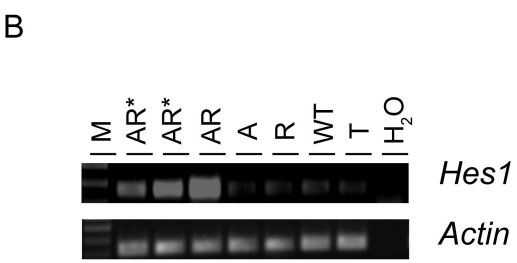
B
M
AR*
AR*
AR
A
R
WT
T
H2O
Hes1
Actin

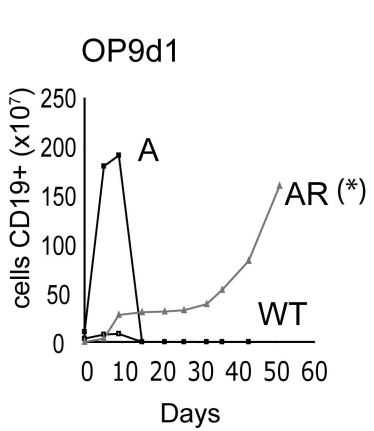
C
OP9d1
cells CD19+ (x10^7)
250
200
150
100
50
0
A
AR (*)
WT
0 10 20 30 40 50 60
Days

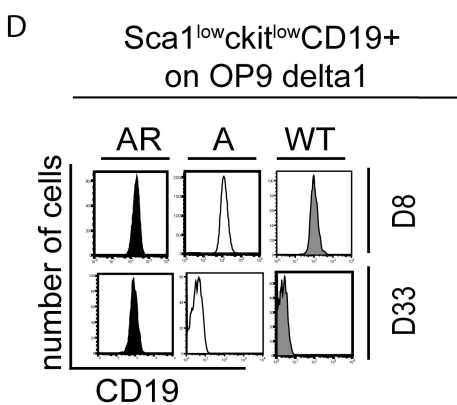
D
Sca1lowckitlowCD19+
on OP9 delta1
AR
A
WT
number of cells
D8
D33
CD19

Figure 5

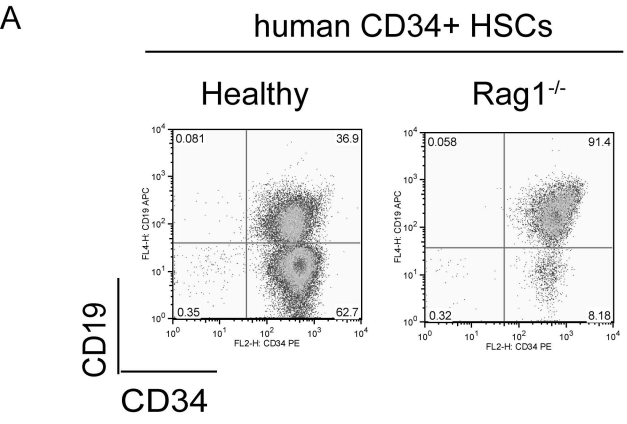
A
human CD34+ HSCs
Healthy
Rag1-/-
0.081
36.9
0.35
62.7
0.058
91.4
0.32
8.18
FL4-H: CD19 APC
FL2-H: CD34 PE
CD19
CD34

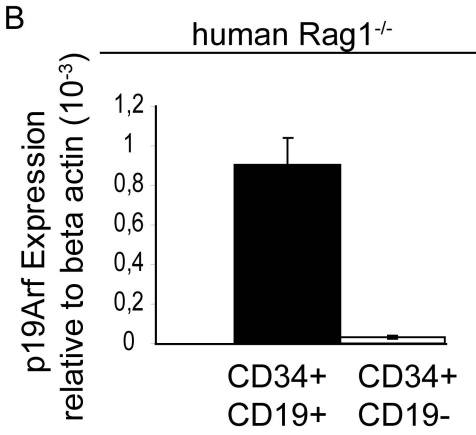
B
human Rag1-/-
p19Arf Expression
relative to beta actin (10-3)
1,2
1
0,8
0,6
0,4
0,2
0
CD34+
CD19+
CD34+
CD19-